

Time Crystal in the Nonlinear Phonon Mode of the Trapped Ions

Yi-Ling Zhan,¹ Chun-Fu Liu,¹ J.-T. Bu,¹ K.-F Cui,^{1,*} S.-L. Su,^{1,2} L.-L. Yan,^{1,2,†} and Gang Chen^{1,‡}

¹*Key Laboratory of Materials Physics, Ministry of Education,
School of Physics and Laboratory of Zhongyuan Light,
Zhengzhou University, Zhengzhou 450001, China*

²*Institute of Quantum Materials and Physics, Henan Academy of Sciences, Zhengzhou 450046, China*

Time crystals constitute a novel phase of matter defined by the spontaneous breaking of time-translation symmetry. We present a scheme for realizing a continuous-time crystal using the vibrational phonon mode of a trapped-ion system. By coupling two addressable standing-wave lasers to individual ions via adiabatic elimination, we generate a nonlinear phonon mode with controllable linear gain (g) and nonlinear damping (κ). This scheme enables stable dissipative dynamics over timescales significantly longer than the oscillation period, leading to the emergence of time-translation symmetry breaking - a time crystal - under specific conditions. Furthermore, we analyze the experimental feasibility and numerically demonstrate this phonon time crystal using experimentally feasible parameters. These results provide a practical scheme for observing a time crystal in a nonlinear phonon mode, which will advance research into time crystals.

I. INTRODUCTION

Time crystals, analogous to conventional spatial crystals, represent a many-body quantum state that spontaneously breaks time-translation symmetry in the ground state. Initially proposed by Wilczek and Shapere [1–3], this concept envisions a system capable of maintaining stable periodic motion without external energy input. However, theoretical studies revealed fundamental constraints: In classical systems with continuous symmetry, the ground state must remain static to prevent energy divergence—a principle termed the “no-go” theorem [4–6]. Consequently, Wilczek’s original model failed to satisfy thermodynamic equilibrium requirements [5].

The concept evolved in 2014 when Krzysztof Sacha introduced discrete time crystals (DTCs) within Floquet systems under periodic driving [7]. By applying an external field with period T , these systems exhibit subharmonic responses with periods nT ($n > 1$, $n \in N^+$) [8], manifesting discrete time-translation symmetry breaking [9]. Notably, even with Hamiltonian perturbations, sufficient Ising interactions enable robust subharmonic responses [10]. Experimental breakthroughs began in 2017 with ion trap observations of period-doubling [11], followed by validations in nitrogen-vacancy centers and superconducting qubits [12–16].

By contrast, continuous time crystals (CTCs), which spontaneously form temporal periodicity without external driving [17–19], better align with Wilczek’s original vision [2]. Their practical advantages in quantum technology spurred research on dissipative time crystals [20–24]. In 2021, researchers at the University of Hamburg first realized dissipative time crystals in a Bose-Einstein condensate coupled to an optical cavity [25], with subsequent demonstrations of CTCs in dissipative systems a year later [26, 27]. This work confirms the feasibility of

circumventing the no-go theorem through environmental coupling and realizing time crystal dynamics [28–32].

Nonlinear systems with limit cycles proving to be a powerful platform for achieving this goal [33, 34]. By introducing linear damping, linear gain, and nonlinear damping, a feasible approach based on nonlinear system is provided [35], where it shows that the system exhibits a metastable state with stable oscillations during its time evolution, accompanied by a dissipative evolution process with a timescale far exceeding the oscillation period. If the dissipation processes can be precisely controlled in experiments, the time crystals can be observed.

As ideal experimental platforms, ion traps enable precise control and exhibit sophisticated engineering characteristics of dissipative mechanisms [36–41]. By tuning laser frequencies and Rabi frequencies, various gain and loss processes can be effectively simulated, establishing ion traps as superb platforms for studying non-equilibrium phenomena [42, 43]. Moreover, their precise single-ion addressing capability ensures experimental accuracy and controllability of dissipative channels across different ions. Another significant advantage lies in high-fidelity measurement techniques, directly implemented through fluorescence detection and quantum projection measurements [44–48], which provide robust data support for investigating time crystal properties.

In this work, we demonstrate the experimental feasibility of realizing the continuous time crystal in the trapped ion system. The rest of this paper is organized as follows: In Sec. II, we choose the appropriate Hamiltonian and Lindblad operators to construct the required scheme for the realization of the time crystals in the trapped ion system. Subsequently, by using the adiabatic elimination method and removing high-frequency terms, we derive an effective Hamiltonian and effective Lindblad operators, which together form the effective Lindblad master equation of time crystals. In Sec. III, we perform a systematic analysis of the practically experimental parameters to validate the consistency of the theoretical scheme and its experimental feasibility. In Sec. IV, we use the feasible parameters to numerically solve the Lindblad master

* cuikaifeng@zzu.edu.cn

† llyan@zzu.edu.cn

‡ chengang971@163.com

equation from a truncated Fock space, and demonstrate the characteristic behavior of time crystals: The system rapidly enters a metastable state with stable oscillations and subsequently evolves toward a steady state, with a decay time significantly longer than the oscillation period. In Sec. V, we discuss the impact of decoherence on time crystals, and the numerical simulation using a thermal state as the initial state has been performed and yields the similar results to those obtained when starting from a vacuum state, which thus demonstrates a remarkable robustness against decoherence of our continuous time crystal and ensures its sustained existence over extended periods. Finally, we give a brief conclusion in Sec. VI.

II. MODEL OF THE SYSTEM

As shown in Fig. 1(a), we consider two $^{40}\text{Ca}^+$ ions trapped in a linear ion trap, where the vibration of ions is driven by an external electric field with strength ε and frequency ω_e . We combine two addressable standing waves of 729 nm laser beams, one global 854 nm traveling laser with σ^+ polarization, and a three-level system (see Fig. 1(b)) to produce different dissipative processes of vibrational phonon mode, where each of lasers serves a distinct purpose: The 854 nm laser is circularly polarized to produce a large effective decay process of two-level system, consisting of the ground state $|0\rangle := |4^2S_{1/2}, m_s = -1/2\rangle$ and metastable state $|1\rangle := |3^2D_{5/2}, m_s = -5/2\rangle$, and two 729 nm laser beams independent of each other different ions induce linear gain with rate g , and nonlinear damping with rate κ , respectively.

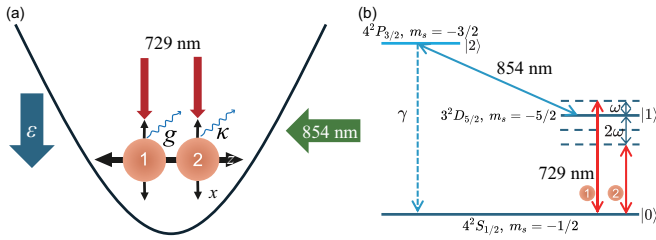


FIG. 1. The schematic of our scheme to realize the time crystal in a trapped $^{40}\text{Ca}^+$ ion system. An external electric field is applied to drive the vibration of ion, an 854 nm laser coupling the metastable state $|1\rangle$ to the excited state $|2\rangle := |4^2P_{3/2}, m_s = -3/2\rangle$ is used to produce a fast decay from the metastable state $|1\rangle$ to the ground state $|0\rangle$, and two standing waves of 729 nm laser beams with different detunings are employed to create linear gain (g) and nonlinear damping (κ) on the vibrational mode, respectively. Here the spontaneous emission rate of excited state is characterized as γ .

The Hamiltonian of the system can be divided into the vibrational mode Hamiltonian H_a and the spin states Hamiltonian H_s . All Hamiltonians in this work are formulated under the condition of $\hbar = 1$, which simplifies the quantum mechanical equations while preserving the

physical consistency of observables. For the vibrational mode, ω_r denotes the frequency of the radial center-of-mass vibrational mode, while a (a^\dagger) represents the corresponding phonon annihilation (creation) operators. The free vibration term of the vibrational mode Hamiltonian is expressed as $\omega_r a^\dagger a$. Since the vibrational mode is driven by an external electric field with strength ε and frequency ω_e , the Hamiltonian must include the external driving term $\varepsilon a e^{i\omega_e t} + \text{h.c.}$. Therefore, the vibrational mode Hamiltonian can be expressed as:

$$H_a = \omega_r a^\dagger a + \varepsilon a e^{i\omega_e t} + \text{h.c.} \quad (1)$$

where the former describes free vibration, and the latter corresponds to the driving by an external electric field.

For the spin states, we can noted that the free energy terms in the Hamiltonian for the metastable state $|1\rangle$ and excited state $|2\rangle$ are given by $\omega_1 |1\rangle_n \langle 1| + \omega_2 |2\rangle_n \langle 2|$, where ω_1 (ω_2) denotes the energy of state $|1\rangle$ ($|2\rangle$). The Rabi frequency and the laser frequency of the 854 nm laser are Ω_e and ω_L^m , respectively. Then we can write coupling Hamiltonian of two ion and globle 854 nm laser beam:

$$H_{854} = \frac{\Omega_e}{2} (\tilde{\sigma}_{-,n} e^{i\omega_L^m t} + \text{h.c.}), \quad (2)$$

the Paul operators are defined as $\tilde{\sigma}_{-,n} = |1\rangle_n \langle 2|$.

The coupling Hamitonian of two ion and two standing waves of 729 nm laser beams is

$$H_{729} = \frac{\bar{\Omega}_n}{2} \left\{ e^{i[\eta(a+a^\dagger)+\phi-\pi/2]} + e^{-i[\eta(a+a^\dagger)+\phi-\pi/2]} \right. \\ \left. \sigma_{-,n} e^{i\omega_L^n t} + \text{h.c.} \right\}, \quad (3)$$

$$= \frac{\Omega_n}{2} \sin[\eta(a+a^\dagger)+\phi] (\sigma_{-,n} e^{i\omega_L^n t} + \text{h.c.}), \quad (4)$$

where the Rabi frequencies, phase, and frequencies of two standing wave 729 nm laser beams are corresponding to $\Omega_n = \bar{\Omega}_n/\sqrt{2}$, ϕ_n , and ω_L^n with $n = 1, 2$. The Lamb-Dicke parameter of 729 nm laser for the two $^{40}\text{Ca}^+$ ions is $\eta = k \cos \alpha / \sqrt{4m\omega_k}$ with the wave vector k of laser, mass of a single ion m and projection angle α between laser and vibrational direction. The Paul operators are defined as $\sigma_{-,n} = |0\rangle_n \langle 1|$.

Rotating into the interaction picture of $H_0 = \omega_e a^\dagger a + \sum_{n=1}^2 (\omega_1 |1\rangle_n \langle 1| + \omega_2 |2\rangle_n \langle 2|)$, the Hamiltonian can be obtained as $H_R = \tilde{H}_a + \tilde{H}_s$ with the Hamiltonians of vibrational mode and spin states corresponding to $\tilde{H}_a = -\Delta a^\dagger a + \varepsilon(a+a^\dagger)$ and

$$\tilde{H}_s = \sum_{n=1}^2 \left\{ \frac{\Omega_e}{2} \tilde{\sigma}_{-,n} e^{i\delta_e t} + \frac{\Omega_n}{2} \sin[\eta(a e^{-i\omega_e t} + a^\dagger e^{i\omega_e t}) \right. \\ \left. + \phi_n] \sigma_{-,n} e^{i\delta_n t} + \text{h.c.} \right\}, \quad (5)$$

where the detunings of 729 nm lasers are corresponding to $\delta_n = \omega_L^n - \omega_1$, the detunings of 854 nm lasers are set same as $\delta_e = \omega_L^e + \omega_1 - \omega_2$ and the detuning of electric field is $\Delta = \omega_e - \omega_r$. To obtain a brief form of efficient

decay rate, we set the 854 nm laser on resonance $\delta_e = 0$ (i.e., $\omega_L^e = \omega_2 - \omega_1$).

The dynamics of the system, following the Markov process, is described by the Lindblad master equation as [49]

$$\dot{\rho} = -i[H_R, \rho] + \sum_{n=1}^2 [2L_n\rho L_n^\dagger - (L_n^\dagger L_n\rho + \rho L_n^\dagger L_n)]/2,$$

where the quantum jump operator of n th ion $L_n = \sqrt{\gamma}|0\rangle_n\langle 2|$ describes the decay path from the excited state $|2\rangle$ of ion to ground state $|0\rangle$ with the decay rate $\gamma/2\pi = 22.4$ MHz. In order to obtain the necessary linear gain and nonlinear damping, we'll use two adiabatic elimination processes.

First, we adiabatically eliminate the excited state $|2\rangle$ to obtain an efficient decay rate from the metastable state $|1\rangle$ to the ground state $|0\rangle$ as (see Appendix A):

$$L_{\text{eff}} = \sum_{n=1}^2 i\sqrt{\Gamma}\sigma_{-,n}, \quad \Gamma = \frac{\Omega_e^2}{\gamma}, \quad (6)$$

where the condition $\gamma \gg \Omega_e \gg \Gamma$ need to be satisfied to ensure the adiabatic elimination of the state $|2\rangle$.

Next, we adiabatically eliminate the metastable state $|1\rangle$ to create the necessary dissipative/gain process on the vibrational mode by selecting the detunings and phases of two 729 nm laser beams as $\phi_1 = 0$, $\delta_1 = \omega_e$, $\phi_2 = \pi/2$ and $\delta_2 = -2\omega_e$, respectively, to produce the linear and nonlinear coupling between the two-level system and the vibrational mode.

Since these two lasers are independent of each other, we first consider the first laser beam, which is given by

$$H_1 = \frac{\Omega_n}{2} \sin[\eta(ae^{i\omega_e t} + a^\dagger e^{i\omega_e t})] \sigma_{-,n} e^{i\delta_n t} + \text{h.c.} \quad (7)$$

If setting $\Omega_1 \ll \omega_e$, expanding the sinusoidal function as a Taylor series and neglecting higher-order terms like $e^{\pm 2i\omega_e t}, e^{\pm 3i\omega_e t}, \dots$, we can obtain

$$\sin[\eta(ae^{-i\omega_e t} + a^\dagger e^{i\omega_e t})] \simeq \tilde{\eta}_1(ae^{-i\omega_e t} + a^\dagger e^{i\omega_e t}), \quad (8)$$

where the effective Lamb-Dicke parameter of ions $\tilde{\eta}_1 = \sum_{k=0}^{\infty} (-n)^k \eta^{2k+1} C_{2k+1}^k / (2k+1)!$ with n denoting the average phonon of vibrational mode and the binomial expansion coefficient $C_{2k+1}^k = (2k+1)!/k!(k+1)!$. Thus, the reduced Hamiltonian is written as

$$H_1 = \frac{\tilde{\eta}_1 \Omega_1}{2} (a\sigma_{-,1} + a^\dagger \sigma_{+,1}). \quad (9)$$

Under the condition $\Gamma \gg \tilde{\eta}_1 \Omega_n$, the state $|1\rangle$ of the first ion can be adiabatically eliminated, yielding the effective Hamiltonian of spin state $H = 0$ and dissipative operators as

$$L_{1,\text{eff}} = -\frac{\tilde{\eta}_1 \Omega_1}{\sqrt{\Gamma}} a^\dagger |0\rangle_1 \langle 0|. \quad (10)$$

Then, we apply the same method to the second laser, where we have $\cos[\eta(ae^{-i\omega_e t} + a^\dagger e^{i\omega_e t})] \simeq \tilde{\eta}_2(a^2 e^{-2i\omega_e t} + (a^\dagger)^2 e^{2i\omega_e t})$ where the effective Lamb-Dicke parameter of ions $\tilde{\eta}_2 = \sum_{k=1}^{\infty} -(-n)^{k-1} \eta^{2k} C_{2k}^{k-1} / (2k)!$. Thus, we get the reduced Hamiltonian as

$$H_2 = \frac{\tilde{\eta}_2 \Omega_2}{2} (a^2 \sigma_{+,2} + (a^\dagger)^2 \sigma_{-,2}), \quad (11)$$

Under the condition $\Gamma \gg \tilde{\eta}_2 \Omega_2$, the state $|1\rangle$ of second ion can be adiabatically eliminated, yielding the effective Hamiltonian of spin state $H = 0$ and dissipative operator as

$$L_{2,\text{eff}} = -\frac{\tilde{\eta}_2 \Omega_2}{\sqrt{\Gamma}} a^2 |0\rangle_2 \langle 0|. \quad (12)$$

By tracing out the spin, we have

$$\dot{\rho} = -i[\tilde{H}_a, \rho] + g\mathcal{D}[a^\dagger]\rho + \kappa\mathcal{D}[a^2]\rho, \quad (13)$$

where the superoperator $\mathcal{D}[o]\rho = o\rho o^\dagger - (o^\dagger o\rho + \rho o^\dagger o)/2$, the linear gain rate $g = \tilde{\eta}_1^2 \Omega_1^2 / \Gamma$ and the nonlinear damping rate $\kappa = \tilde{\eta}_2^2 \Omega_2^2 / \Gamma$, respectively.

III. EXPERIMENTAL FEASIBILITY

For the trapped $^{40}\text{Ca}^+$ ion system, the life time of excited state $4^2P_{3/2}$ is 6.9 ns, which gives a decay rate $\gamma/2\pi = 22.4$ MHz [39]. The trap frequency is accessible in an interval $\omega_t/2\pi \in [0.1, 10]$ MHz [50]. The 854 nm laser can drive a dipole transition between the metastable state and the excited state which produces a Rabi frequency of several MHz, even tens of MHz. The 729 nm laser drives a quadrupole transition between the metastable state and the ground state. Its maximal Rabi frequency is generally around several hundred kHz and rarely reaches the MHz level [50]. Particularly, the Lamb-Dicke parameter of $^{40}\text{Ca}^+$ is $\eta \approx 0.1$ under a trap frequency of $\omega_t/2\pi = 1$ MHz for a single ion. As the number of ions (N) increases, η diminishes proportionally to $1/\sqrt{N}$ due to collective vibrational modes. Consequently, for the axial center-of-mass mode of two ions, the parameter ranges as $\eta \in [0.022, 0.22]$ when the trap frequency is tuned within $\omega_t/2\pi \in [0.1, 10]$ MHz to optimize ion coupling.

To obtain the effective Hamiltonian, linear gain, and nonlinear damping processes of the vibrational mode, we have to make two adiabatic approximations and neglect higher-order terms in the above discussion. Combining these two approximation processes, the parameters in the Schrödinger picture should satisfy the following relation

$$\gamma \gg \Omega_e, \omega_r \gg \Gamma \gg \tilde{\eta}_n \Omega_n \gg \varepsilon, \kappa, g \quad (14)$$

with $n = 1, 2$. Since the effective Lamb-Dicke parameter $\tilde{\eta}_1 \propto \eta$, the effective Rabi frequencies ($\tilde{\eta}_n \Omega_n$) produced by the first and second 729 nm lasers are general smaller than 30 kHz. Meanwhile, because of $\tilde{\eta}_2 \propto \eta^2$, the effective Rabi frequency produced by the second 729 nm lasers is general smaller than 2 kHz.

To simple the process of demonstrating the time crystal of vibrational mode, we choose the frequency of axial center-of-mass mode as $\omega_r/2\pi = 1$ MHz (the trapped frequency along the radial direction $\omega_t/2\pi = \sqrt{2}$ MHz), giving the Lamb-Dicke parameter $\eta = 0.07$. The detuning of external electric field $\Delta/2\pi = 5$ kHz, the Rabi frequency of 854 nm laser as $\Omega_e/2\pi = 1.34$ MHz which gives an effective decay rate $\Gamma/2\pi = 80$ kHz. In our

scheme, we choose the vibrational ground state as the initial state for the evolution and obtain the approximate effective Lamb-Dicke parameters about $\tilde{\eta}_1 \approx 0.066$ and $\tilde{\eta}_2 \approx 0.0018$. Then, the Rabi frequencies of the first 729 nm laser are chosen as $\Omega_1/2\pi = 100$ kHz which produce the $g/2\pi = 0.54$ kHz, respectively. Besides, we explore the system's dynamics under different nonlinear damping rates by varying the Rabi frequency of the second laser Ω_2 . To investigate the intrinsic dynamics of the system, we perform numerical simulations under the ideal condition where the decoherence induced by the noise and environment are ignored.

IV. PHONON TIME CRYSTAL OF VIBRATIONAL MODE

A. Classical driven Van der Pol oscillator model

To further understand the dynamics of the quantum system, we first examine the following classical model. Considering the thermodynamic limit, the Lindblad master equation can be further reduced to a driven Van der Pol oscillator model, where the evolution of amplitude $\alpha = \langle a \rangle$ is described by the following differential equation (see Appendix B)

$$\dot{\alpha} = \left(\frac{g}{2} + i\Delta - \kappa|\alpha|^2 \right) \alpha - i\varepsilon, \quad (15)$$

which exhibits both Hopf bifurcation and a limit cycle phase [51–54]. The Hopf bifurcation point is characterized by the rescaled driving strength parameter

$$\varepsilon\sqrt{\kappa} = \frac{\sqrt{g(g^2 + 4\Delta^2)}}{4}, \quad (16)$$

in the limit of $\kappa \rightarrow 0$ [55]. This classical model is well studied and we focus on investigating the nonequilibrium behavior at the full quantum level, especially in the phonon mode of a quantum harmonic oscillator.

B. Phonon time crystal of ions

To study the evolution of phonon number and purity, we numerically solve the time evolution of the vibrational mode in the Fock basis. In Fig. 2(a), we demonstrate the temporal evolution of the rescaled photon number [56], defined as $\Omega_2^2 N_a = \Omega_2^2 \langle a^\dagger a \rangle$, for three distinct values of Ω_2 . As the parameter Ω_2 decreases, the associated nonlinear damping rate becomes weaker, which results in two notable changes: an increase in the amplitude of oscillations and a lengthening of the relaxation time. These observations highlight the dynamic behavior of the system as it transitions through different regimes. The oscillatory nature of the evolution provides strong evidence for the dissipative gap closing in the thermodynamic limit, thereby confirming that the vibrational mode behaves as a time crystal. We also plot the classical time evolution

curve governed by Eq. (15), starting from $\alpha = 0$. As Ω_2 decreases, the nonlinear damping rate also decreases, and the time evolution at the quantum level approaches that of the classical time evolution.

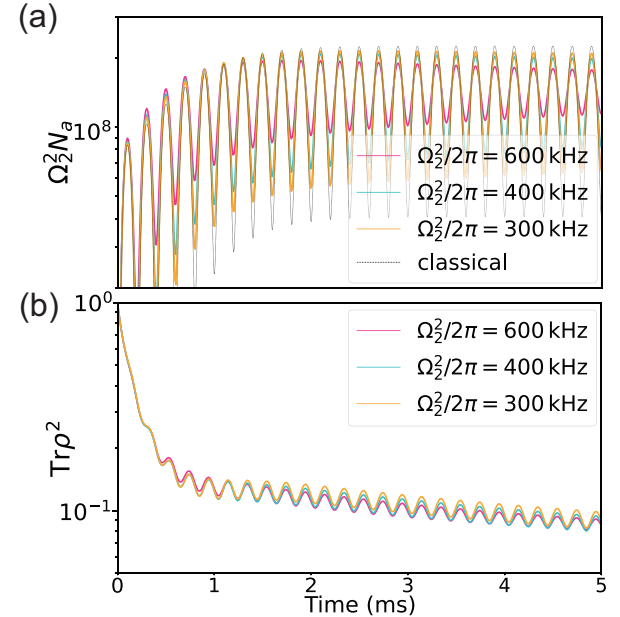


FIG. 2. The time evolution of (a) the rescaled photon number $\Omega_2 N_a$ and (b) the purity $\text{Tr}\rho^2$, where the black dashed line in panel (a) represents the time evolution of the classical model. The initial state of the vibrational mode is the vacuum state and the rescaled driving strength is chosen as $\varepsilon\sqrt{\kappa} \approx 0.0018\varepsilon\Omega_3\sqrt{\gamma}/\Omega_e = 14.27$ kHz $^{3/2}$, where $\Omega_3/2\pi$ takes values of 600 kHz, 400 kHz, and 300 kHz, respectively. Here, the other parameters are chosen by the accessible parameters provided the main text as $\Delta/2\pi = 5$ kHz, $\Omega_2/2\pi = 100$ kHz and $\Omega_e/2\pi = 1.34$ MHz, respectively.

In addition to examining the rescaled photon number, as shown in Fig. 2(b), we also analyze the time-dependent evolution of the state purity. The system is initialized in the vibrational ground state, characterized by a purity of $\text{Tr}\rho^2 = 1$. At the beginning of the evolution, the purity drops rapidly due to interactions within the system. After this initial decrease, the system enters a metastable state where the purity stabilizes temporarily, before oscillations set in. Over time, the oscillations gradually dampen, and the system approaches a steady-state value of purity.

C. Husimi Q Function Analysis

Next, we will study the evolution process of Husimi Q function defined as $Q(\alpha) = \langle \alpha | \rho | \alpha \rangle / \pi$, where ρ is the density matrix of the quantum state and $|\alpha\rangle$ is a coherent state in phase space with the complex number $\alpha = q + ip$ corresponding to a specific point in phase space [57]. The Husimi Q function provides a quasi-classical representation of the quantum state, allowing us to intuitively understand how the quantum state is distributed in the

classical phase space. And it also provides a quasiprobability distribution and its maximal value can partially reflect the phase fluctuation of the quantum oscillation.

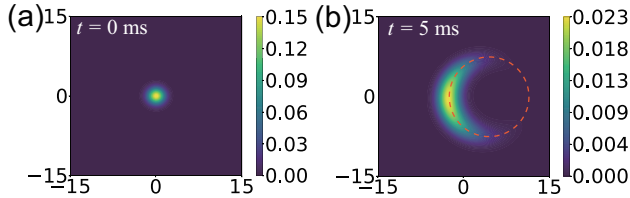


FIG. 3. Quantum Husimi distribution at $t = 0$ ms (a) and $t = 5$ ms (b). The red dashed line represents the limit cycle. The Ω_2 is chosen as $\Omega_3/2\pi = 300$ kHz and other parameters are the same as in Fig. 2.

Similar to the evolution of state purity, starting from the initial vacuum state, there is a rapid dephasing process at beginning, followed by a slowdown in the rate of dephasing, and then continuously oscillations [51]. Eventually, the oscillations gradually fade, and the quantum limit cycle becomes blurred. In Fig. 3(a) and 3(b), we illustrate the evolution of the Q function: Initially, the Q function appears as a Gaussian wave packet, reflecting the coherence of the initial state, which aligns with the initial state of our setup, i.e., the vacuum state. As the evolution progresses, the Q function gradually disperses, with the wave packet rotating along the limit cycle in phase space and becoming increasingly elongated.

V. ROBUSST TO THE THERMAL EFFECT

In the practical experiments, the system cannot always be prepared in the vacuum state as described in Sec. IV or an ideal coherent state, but the state of the system more generally evolves into a thermal state with an effective temperature. Consequently, the impact of thermal effects on the evolution of the time crystal will be considered. Fortunately, our model demonstrates remarkable robustness against decoherence. As a result, we are able to directly use the thermal state as the initial condition. To discuss the thermal effect, we assume that we initially prepare the vibrational mode in a thermal state $\rho_{\text{th}} = \exp(-\beta H_{r0})/\text{Tr}[\exp(-\beta H_{r0})]$ with the inverse temperature $\beta = 1/k_B T$ (k_B is the Boltzmann constant and T is the effective temperature of vibrational state) and Hamiltonian of vibrational mode $H_{r0} = \hbar\omega_r a^\dagger a$ [58, 59]. This state gives an average phonon number $\bar{n}_0 = \langle n \rangle = 1/(e^{\beta\hbar\omega_r} - 1)$ and a probability distribution on the Fock state as $p_n = \bar{n}_0^n / (\bar{n}_0 + 1)^{n+1}$.

In Fig. 4 and 5, we discuss the evolution of the vibrational mode under three thermal states with the average photon numbers of 0 (vacuum state), 5, and 10 as the initial states. We first investigated the evolution of the rescaled photon number, as shown in Fig. 4. It can be observed that the choice of the thermal state does not affect the oscillation period of the time crystal but only leads to changes in the amplitude.

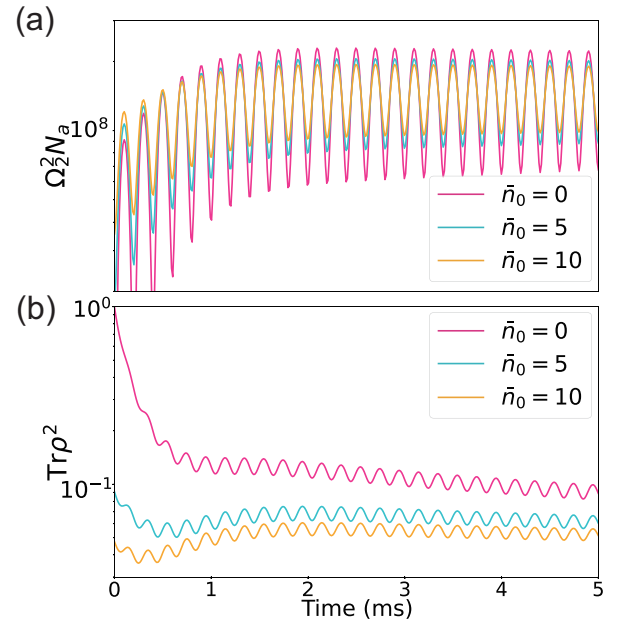


FIG. 4. The rescaled photon number (a) and purity (b) for the evolution with thermal states as the initial states, where the initial thermal states are assumed with the average photon numbers of $\bar{n}_0 = 0, 5$ and 10 . The other parameters we choose are the same as in Fig. 3

Due to the difficulty of measuring the photon number distribution and purity in the practical experiments, we plot the evolution of the population in different Fock states with an initial thermal state. By selecting evolution time t between 2.5 ms and 3.75 ms, we can clearly observe the oscillatory behavior of the population in Fig. 5. Thus, by setting different thermal state as the initial state, we observe that the time crystals of phonon modes show strong robustness against thermal effects, being able to maintain their spontaneous breaking of time symmetry and enabling them to persist for long periods of time.

VI. CONCLUSION

In summary, we have constructed a continuous-time crystal in a linear ion trap by employing a system of two ions. Compared to existing methods for implementing discrete-time crystals in ion traps, our scheme offers enhanced stability for the time crystal behavior. Based on the practical parameters and detailed numerical simulations, we have verified the experimental feasibility of this scheme and observed the time-dependent evolution results for the system's phonon number, purity, and Q -function under ideal conditions, confirming the existence of the time crystal. Furthermore, through the use of different thermal states as initial conditions, we demonstrate that our continuous-time crystal model exhibits remarkable robustness against thermal effects. Our findings provide a feasible approach for constructing time

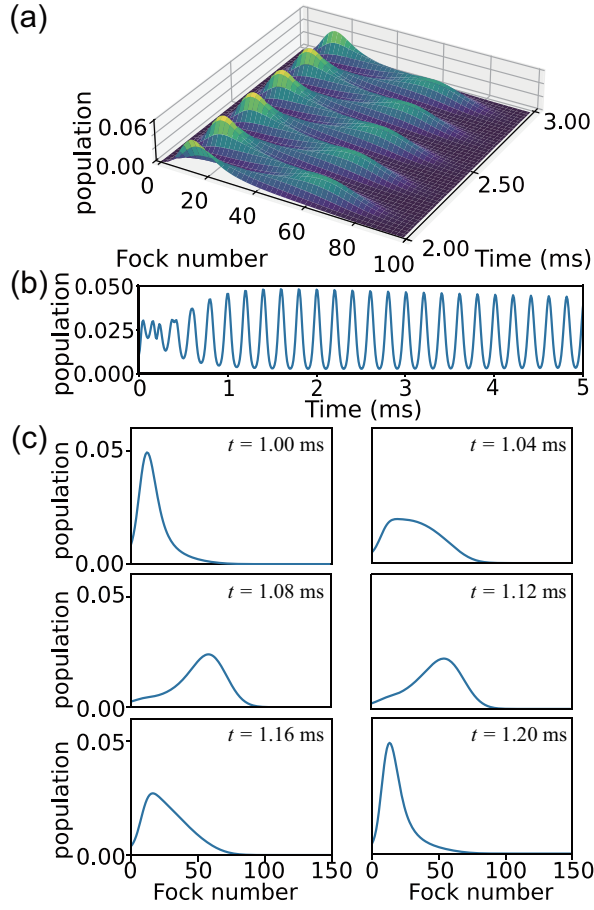


FIG. 5. The evolution of population in the Fock states for the thermal state with an average phonon $\bar{n}_0 = 5$. (a) The evolution of the population in different Fock states between 2.0 ms to 3.0 ms. (b) Evolution of the population in the Fock state $|15\rangle$. (c) The population in different Fock states at six equally time division points within the time range from $t = 2.5\text{ms}$ to $t = 2.75\text{ms}$. The parameters are chosen as the same as those in Fig. 3 and Fig. 4.

crystals and offer valuable insights for research in many-body physics and non-equilibrium thermodynamics.

ACKNOWLEDGMENTS

This work is supported by the National Key Research and Development Program of China under Grant Nos. 2022YFA1404500 and 2021YFA1400902, by Cross-disciplinary Innovative Research Group Project of Henan Province under Grant No. 232300421004, National Natural Science Foundation of China under Grant Nos. 1232410, U21A20434, 12074346, 12274376, 12374466, 12074232, 12125406, by Natural Science Foundation of Henan Province under Grant Nos. 232300421075, 242300421212, by Major science and technology project of Henan Province under Grant No. 221100210400.

Appendix A: Adiabatic Elimination of Spin States

The density matrix ρ of the system can be described by the Lindblad master equation as

$$\dot{\rho} = -i[H_R, \rho] + \frac{1}{2} \sum_{n=1}^2 [2L_n \rho L_n^\dagger - (L_n^\dagger L_n \rho + \rho L_n^\dagger L_n)],$$

with dissipative operator $L_n = \sqrt{\gamma}|0\rangle_n\langle 2|$. Our aim is to reduce the system's dynamics to an effective master equation that only involves the vibrational mode. Thus, we use the effective operator formalism in Ref. [60] to adiabatic eliminate the spin of system, where the effective dynamics of methods provided in Ref. [60] can be described as

$$\dot{\rho} = -i[H_{\text{eff}}, \rho] + \frac{1}{2} \sum_{n=1}^2 \mathcal{D}[L_{n,\text{eff}}]\rho, \quad (\text{A1})$$

where the effective Hamiltonian and Lindblad operators are given as

$$H_{\text{eff}} = -\frac{1}{2}V_- [H_{\text{NH}}^{-1} + (H_{\text{NH}}^{-1})^\dagger] V_+ + H_g, \quad (\text{A2})$$

$$L_{n,\text{eff}}^k = L_n H_{\text{NH}}^{-1} V_+, \quad (\text{A3})$$

where V_+ (V_-) are the coupling terms between the excited-state subspace and ground-state subspace of system, H_g is the Hamiltonian of the ground-state subspace, and H_{NH} is the non-Hermitian Hamiltonian

$$H_{\text{NH}} = H_e - \frac{i}{2} \sum_k L_k^\dagger L_k, \quad (\text{A4})$$

with H_e being the Hamiltonian of the excited-state subspace. During this adiabatic elimination process, it needs that the dynamics of excited-state subspace should be much faster than the dynamics of ground-state subspace and the coupling dynamics between them, and the coupling dynamics between them should be much faster than the dynamics of ground-state subspace.

First, we eliminate the excited state $|2\rangle$ of ions. In this situation, the original Hamiltonian are defined as $H_R = H_g + H_e + V_- + V_+$ where $H_g = \tilde{H}_a + H_d$ with $H_d = \sum_{n=1}^2 \Omega_n \{ \sin[\eta(ae^{-i\omega_e t} + a^\dagger e^{i\omega_e t}) + \phi_n] \sigma_{-,n} e^{i\delta_n t} + \text{h.c.} \}$, $H_e = 0$, $V_- = \sum_{n=1}^2 \Omega_e \tilde{\sigma}_{-,n} / 2$ and $V_+ = \sum_{n=1}^2 \Omega_e \tilde{\sigma}_{+,n} / 2$, and the Lindblad operators are given as $L_n = \sqrt{\gamma}|0\rangle_n\langle 2|$. From Eq. (A4), we can obtain

$$H_{\text{NH}} = -\frac{i\gamma}{2} \sum_{n=1}^2 |2\rangle_n\langle 2|, \quad H_{\text{NH}}^{-1} = \frac{2i}{\gamma} \sum_{n=1}^2 |2\rangle_n\langle 2|, \quad (\text{A5})$$

which result into

$$H_{\text{eff}} = H_g, \quad L_{n,\text{eff}} = i \frac{\Omega_e}{\sqrt{\gamma}} \sigma_{-,n}, \quad (\text{A6})$$

giving an effective decay rate $\Gamma = \Omega_e^2/\gamma$ from the metastable state $|1\rangle$ to ground state $|0\rangle$. Moreover, the constraint conditions for adiabatic elimination mean that $\gamma \gg \Omega_e \gg \Gamma, \Omega_n, \varepsilon$.

Using the same method, we can then eliminate the metastable state $|1\rangle$ to produce the necessary damping processes on the vibrational mode. In this adiabatic elimination process, we have

$$H_g = \tilde{H}_a, \quad H_e = 0, \quad (\text{A7})$$

$$V_+ = \frac{\tilde{\eta}_1 \Omega_1}{2} a^\dagger \sigma_{+,1} + \frac{\tilde{\eta}_2 \Omega_2}{2} a^2 \sigma_{+,2}, \quad (\text{A8})$$

$$V_- = \frac{\tilde{\eta}_1 \Omega_1}{2} a \sigma_{-,1} + \frac{\tilde{\eta}_2 \Omega_2}{2} (a^2)^\dagger \sigma_{-,2}, \quad (\text{A9})$$

which then give

$$H_{\text{NH}} = -\frac{i\Gamma}{2} \sum_{n=1}^2 |1\rangle_n \langle 1|, \quad H_{\text{NH}}^{-1} = \frac{2i}{\Gamma} \sum_{n=1}^2 |1\rangle_n \langle 1|, \quad (\text{A10})$$

and finally obtain

$$H_{\text{eff}} = \tilde{H}_a, \quad (\text{A11})$$

$$L_{1,\text{eff}} = -\frac{\tilde{\eta}_1 \Omega_1}{\sqrt{\Gamma}} a^\dagger |0\rangle_1 \langle 0|, \quad L_{2,\text{eff}} = -\frac{\tilde{\eta}_2 \Omega_2}{\sqrt{\Gamma}} a^2 |0\rangle_2 \langle 0|,$$

which give the effective linear gain rate $g = \tilde{\eta}_1^2 \Omega_1^2 / \Gamma$ and the effective nonlinear damp rate $\kappa = \tilde{\eta}_2^2 \Omega_2^2 / \Gamma$. Besides, the constraint conditions of adiabatic elimination can be obtained as $\Gamma \gg \tilde{\eta}_1^2 \Omega_1, \tilde{\eta}_2^2 \Omega_2 \gg g, \kappa, \varepsilon$.

Appendix B: Classical Van der Pol model

For our purpose, we reduce the Lindblad master equation in Eq. (13) to the equation for the amplitude $\alpha = \langle a \rangle$ in Eq. (15). To achieve this, we can right-multiply both sides of Eq. (13) by the annihilation operator a and then take the trace over it, giving it as

$$\begin{aligned} \text{Tr}\{\dot{\rho}a\} &= -i\text{Tr}\{[H_a, \rho]a\} \\ &\quad + \text{Tr}\{g\mathcal{D}[a^\dagger]\rho a\} + \text{Tr}\{\kappa\mathcal{D}[a^2]\rho a\}. \end{aligned} \quad (\text{B1})$$

Substituting $H_a = -\Delta a^\dagger a + \varepsilon a^\dagger + \varepsilon^* a$ into the above equation, we obtain

$$-\text{Tr}\{[H_a, \rho]a\} = \Delta\alpha - \varepsilon, \quad (\text{B2})$$

where we use the relation $a^\dagger a = aa^\dagger - 1$ and the cyclic property of the trace. Similarly, the gain and damping terms $\text{Tr}\{g\mathcal{D}[a^\dagger]\rho a\}$ and $\text{Tr}\{\kappa\mathcal{D}[a^2]\rho a\}$ can be rewritten as

$$\begin{aligned} \text{Tr}\{g\mathcal{D}[a^\dagger]\rho a\} &= \frac{g}{2} \text{Tr}\{\rho a^2 a^\dagger - \rho a a^\dagger a\} = \frac{g}{2}\alpha, \\ \text{Tr}\{\kappa\mathcal{D}[a^2]\rho a\} &= \frac{\lambda}{2} \text{Tr}[\rho(a^\dagger)^2 a^3 - \rho a(a^\dagger)^2 a^2] = -\lambda|\alpha|^2\alpha. \end{aligned} \quad (\text{B3})$$

Consequently, we arrive at the following expression:

$$\dot{\alpha} = \left(\frac{g - \kappa}{2} + i\Delta \right) \alpha - \lambda|\alpha|^2\alpha - i\varepsilon, \quad (\text{B4})$$

where $\varepsilon\sqrt{\lambda}$ is a constant.

[1] A. Shapere and F. Wilczek, Classical time crystals, *Phys. Rev. Lett.* **109**, 160402 (2012).

[2] F. Wilczek, Quantum time crystals, *Phys. Rev. Lett.* **109**, 160401 (2012).

[3] F. Wilczek, Superfluidity and space-time translation symmetry breaking, *Phys. Rev. Lett.* **111**, 250402 (2013).

[4] P. Bruno, Comment on “quantum time crystals”, *Phys. Rev. Lett.* **110**, 118901 (2013).

[5] P. Bruno, Impossibility of spontaneously rotating time crystals: A no-go theorem, *Phys. Rev. Lett.* **111**, 070402 (2013).

[6] H. Watanabe and M. Oshikawa, Absence of quantum time crystals, *Phys. Rev. Lett.* **114**, 251603 (2015).

[7] K. Sacha, Modeling spontaneous breaking of time-translation symmetry, *Phys. Rev. A* **91**, 033617 (2015).

[8] V. Khemani, A. Lazarides, R. Moessner, and S. L. Sondhi, Phase structure of driven quantum systems, *Phys. Rev. Lett.* **116**, 250401 (2016).

[9] D. V. Else, C. Monroe, C. Nayak, and N. Y. Yao, Discrete time crystals, *Annu. Rev. Condens. Matter Phys.* **11**, 467 (2020).

[10] N. Y. Yao, A. C. Potter, I.-D. Potirniche, and A. Vishwanath, Discrete time crystals: Rigidity, criticality, and realizations, *Phys. Rev. Lett.* **118**, 030401 (2017).

[11] H. P. W. Zhang, J. A. Kyprianidis, P. Becker, A. Lee, J. Smith, G. Pagano, I.-D. Potirniche, A. C. Potter, A. Vishwanath, N. Y. Yao, and C. Monroe, Observation of a discrete time crystal, *Nature* **543**, 217 (2017).

[12] S. Choi, J. Choi, R. Landig, G. Kucsko, H. Zhou, J. Isoya, F. Jelezko, S. Onoda, H. Sumiya, V. Khemani, C. von Keyserlingk, N. Y. Yao, E. Demler, and M. D. Lukin, Observation of discrete time-crystalline order in a disordered dipolar many-body system, *Nature* **543**, 221 (2017).

[13] W. W. Ho, S. Choi, M. D. Lukin, and D. A. Abanin, Critical time crystals in dipolar systems, *Phys. Rev. Lett.* **119**, 010602 (2017).

[14] X. Mi, M. Ippoliti, C. Quintana, A. Greene, Z. Chen, J. Gross, F. Arute, K. Arya, J. Atalaya, R. Babbush, J. C. Bardin, J. Basso, A. Bengtsson, A. Bilmes, A. Bourassa, L. Brill, M. Broughton, B. B. Buckley, D. A. Buell, B. Burkett, N. Bushnell, B. Chiaro, R. Collins, W. Courtney, D. Debroy, S. Demura, A. R. Derk, A. Dunsworth, D. Eppens, C. Erickson, E. Farhi, A. G. Fowler, B. Foxen, C. Gidney, M. Giustina, M. P. Harrigan, S. D. Harrington, J. Hilton, A. Ho, S. Hong, T. Huang, A. Huff, W. J. Huggins, L. B. Ioffe, S. V. Isakov, J. Iveland, E. Jeffrey, Z. Jiang, C. Jones, D. Kafri, T. Khattar, S. Kim, A. Kitaev, P. V. Klimov, A. N. Korotkov, F. Kostritsa, D. Landhuis, P. Laptev, J. Lee, K. Lee, A. Locharla, E. Lucero, O. Martin,

J. R. McClean, T. McCourt, M. McEwen, K. C. Miao, M. Mohseni, S. Montazeri, W. Mruczkiewicz, O. Naaman, M. Neeley, C. Neill, M. Newman, M. Y. Niu, T. E. O'Brien, A. Opremcak, E. Ostby, B. Pato, A. Petukhov, N. C. Rubin, D. Sank, K. J. Satzinger, V. Shvarts, Y. Su, D. Strain, M. Szalay, M. D. Trevithick, B. Villalonga, T. White, Z. J. Yao, P. Yeh, J. Yoo, A. Zalcman, H. Neven, S. Boixo, V. Smelyanskiy, A. Megrant, J. Kelly, Y. Chen, S. L. Sondhi, R. Moessner, K. Kechedzhi, V. Khemani, and P. Roushan, Time-crystalline eigenstate order on a quantum processor, *Nature* **601**, 531 (2022).

[15] P. Frey and S. Rachel, Realization of a discrete time crystal on 57 qubits of a quantum computer, *Science Advances* **8**, eabm7652 (2022).

[16] H. Wang, Y.-J. Zhao, H.-C. Sun, X.-W. Xu, Y. Li, Y. Zheng, Q. Liu, and R. Li, Controlling the qubit-qubit coupling in the superconducting circuit with double-resonator couplers, *Phys. Rev. A* **109**, 012601 (2024).

[17] V. K. Kozin and O. Kyriienko, Quantum time crystals from hamiltonians with long-range interactions, *Phys. Rev. Lett.* **123**, 210602 (2019).

[18] A. Greilich, N. E. Kopteva, A. N. Kamenskii, P. S. Sokolov, V. L. Korenev, and M. Bayer, Robust continuous time crystal in an electron-nuclear spin system, *Nat. Phys.* **20**, 631 (2024).

[19] N. I. Zheludev and K. F. MacDonald, Realization of a continuous time crystal in a photonic metamaterial, *Nat. Phys.* **19**, 939 (2023).

[20] F. Iemini, A. Russomanno, J. Keeling, M. Schirò, M. Dalmonte, and R. Fazio, Boundary time crystals, *Phys. Rev. Lett.* **121**, 035301 (2018).

[21] Z. Gong, R. Hamazaki, and M. Ueda, Discrete time-crystalline order in cavity and circuit qed systems, *Phys. Rev. Lett.* **120**, 040404 (2018).

[22] F. M. Gambetta, F. Carollo, M. Marcuzzi, J. P. Garrahan, and I. Lesanovsky, Discrete time crystals in the absence of manifest symmetries or disorder in open quantum systems, *Phys. Rev. Lett.* **122**, 015701 (2019).

[23] B. Buča and D. Jaksch, Dissipation induced nonstationarity in a quantum gas, *Phys. Rev. Lett.* **123**, 260401 (2019).

[24] B. Buča, J. Tindall, and D. Jaksch, Non-stationary coherent quantum many-body dynamics through dissipation, *Nat. Commun.* **10**, 1730 (2019).

[25] H. Keßler, P. Kongkhambut, C. Georges, L. Mathey, J. G. Cosme, and A. Hemmerich, Observation of a dissipative time crystal, *Phys. Rev. Lett.* **127**, 043602 (2021).

[26] P. Kongkhambut, J. Skulte, L. Mathey, J. G. Cosme, A. Hemmerich, and H. Keßler, Observation of a continuous time crystal, *Science* **377**, 670 (2022).

[27] L. J. LeBlanc, Unleashing spontaneity in a time crystal, *Science* **377**, 576 (2022).

[28] Y.-X. Xiang, Q.-L. Lei, Z. Bai, and Y.-Q. Ma, Self-organized time crystal in driven-dissipative quantum system, *Phys. Rev. Res.* **6**, 033185 (2024).

[29] D. Chen, Z. Peng, J. Li, S. Chesi, and Y. Wang, Discrete time crystal in an open optomechanical system, *Phys. Rev. Res.* **6**, 013130 (2024).

[30] A. Riera-Campeny, M. Moreno-Cardoner, and A. Sanpera, Time crystallinity in open quantum systems, *Quantum* **4**, 270 (2020).

[31] B. Das, N. Jaseem, and V. Mukherjee, Discrete time crystals in the presence of non-markovian dynamics, *Phys. Rev. A* **110**, 012208 (2024).

[32] A. Lazarides, S. Roy, F. Piazza, and R. Moessner, Time crystallinity in dissipative floquet systems, *Phys. Rev. Res.* **2**, 022002 (2020).

[33] M. Krishna, P. Solanki, M. Hajdušek, and S. Vinjanampathy, Measurement-induced continuous time crystals, *Phys. Rev. Lett.* **130**, 150401 (2023).

[34] X. Wu, Z. Wang, F. Yang, R. Gao, C. Liang, M. K. Tey, X. Li, T. Pohl, and L. You, Dissipative time crystal in a strongly interacting rydberg gas, *Nat. Phys.* **20**, 1389 (2024).

[35] Y. Li, C. Wang, Y. Tang, and Y.-C. Liu, Time crystal in a single-mode nonlinear cavity, *Phys. Rev. Lett.* **132**, 183803 (2024).

[36] A. Bermudez, T. Schaetz, and M. B. Plenio, Dissipation-assisted quantum information processing with trapped ions, *Phys. Rev. Lett.* **110**, 110502 (2013).

[37] X.-Q. Shao, Engineering steady entanglement for trapped ions at finite temperature by dissipation, *Phys. Rev. A* **98**, 042310 (2018).

[38] D. C. Cole, J. J. Wu, S. D. Erickson, P.-Y. Hou, A. C. Wilson, D. Leibfried, and F. Reiter, Dissipative preparation of w states in trapped ion systems, *New J. Phys.* **23**, 073001 (2021).

[39] L.-L. Yan, J.-W. Zhang, M.-R. Yun, J.-C. Li, G.-Y. Ding, J.-F. Wei, J.-T. Bu, B. Wang, L. Chen, S.-L. Su, F. Zhou, Y. Jia, E.-J. Liang, and M. Feng, Experimental verification of dissipation-time uncertainty relation, *Phys. Rev. Lett.* **128**, 050603 (2022).

[40] T. Behrle, T. L. Nguyen, F. Reiter, D. Baur, B. de Neeve, M. Stadler, M. Marinelli, F. Lancellotti, S. F. Yelin, and J. P. Home, Phonon laser in the quantum regime, *Phys. Rev. Lett.* **131**, 043605 (2023).

[41] L.-L. Yan, J.-T. Bu, Q. Zeng, K. Zhang, K.-F. Cui, F. Zhou, S.-L. Su, L. Chen, J. Wang, G. Chen, and M. Feng, Experimental verification of demon-involved fluctuation theorems, *Phys. Rev. Lett.* **133**, 090402 (2024).

[42] H. C. Nägerl, D. Leibfried, H. Rohde, G. Thalhammer, J. Eschner, F. Schmidt-Kaler, and R. Blatt, Laser addressing of individual ions in a linear ion trap, *Phys. Rev. A* **60**, 145 (1999).

[43] S. Charles Doret, J. M. Amini, K. Wright, C. Volin, T. Killian, A. Ozakin, D. Denison, H. Hayden, C.-S. Pai, R. E. Slusher, and A. W. Harter, Controlling trapping potentials and stray electric fields in a micro-fabricated ion trap through design and compensation, *New J. Phys.* **14**, 073012 (2012).

[44] W. J. Setzer, M. Ivory, O. Slobodyan, J. W. Van Der Wall, L. P. Parazzoli, D. Stick, M. Gehl, M. G. Blain, R. R. Kay, and H. J. McGuinness, Fluorescence detection of a trapped ion with a monolithically integrated single-photon-counting avalanche diode, *Appl. Phys. Lett.* **119**, 154002 (2021).

[45] P. Schindler, D. Nigg, T. Monz, J. T. Barreiro, E. Martinez, S. X. Wang, S. Quint, M. F. Brandl, V. Nebendahl, C. F. Roos, M. Chwalla, M. Hennrich, and R. Blatt, A quantum information processor with trapped ions, *New J. Phys.* **15**, 123012 (2013).

[46] K. Okada, M. Wada, T. Nakamura, T. Takayanagi, I. Katayama, and S. Ohtani, Space-charge shift in motional resonance of ca+ induced by simultaneously trapped molecular ions in linear paul trap, *Jpn. J. Appl. Phys.* **45**, 951 (2006).

[47] Z. Fei, X. Yi, X. You-Yang, L. Jiao-Mei, H. Xue-Ren, and F. Mang, Control of a cloud of laser-cooled 40ca+ in

a linear ion trap, *Chin. Phys. Lett.* **27**, 043201 (2010).

[48] S. Ding, G. Maslennikov, R. Hablützel, and D. Matsukevich, Cross-kerr nonlinearity for phonon counting, *Phys. Rev. Lett.* **119**, 193602 (2017).

[49] G. Lindblad, On the generators of quantum dynamical semigroups, *Commun. Math. Phys.* **48**, 119 (1976).

[50] C. Monroe, W. C. Campbell, L.-M. Duan, Z.-X. Gong, A. V. Gorshkov, P. W. Hess, R. Islam, K. Kim, N. M. Linke, G. Pagano, P. Richerme, C. Senko, and N. Y. Yao, Programmable quantum simulations of spin systems with trapped ions, *Rev. Mod. Phys.* **93**, 025001 (2021).

[51] C. Navarrete-Benlloch, T. Weiss, S. Walter, and G. J. de Valcárcel, General linearized theory of quantum fluctuations around arbitrary limit cycles, *Phys. Rev. Lett.* **119**, 133601 (2017).

[52] L. Ben Arosh, M. C. Cross, and R. Lifshitz, Quantum limit cycles and the rayleigh and van der pol oscillators, *Phys. Rev. Res.* **3**, 013130 (2021).

[53] T. Weiss, S. Walter, and F. Marquardt, Quantum-coherent phase oscillations in synchronization, *Phys. Rev. A* **95**, 041802 (2017).

[54] S. Sonar, M. Hajdušek, M. Mukherjee, R. Fazio, V. Vedral, S. Vinjanampathy, and L.-C. Kwek, Squeezing enhances quantum synchronization, *Phys. Rev. Lett.* **120**, 163601 (2018).

[55] W. Casteels, R. Fazio, and C. Ciuti, Critical dynamical properties of a first-order dissipative phase transition, *Phys. Rev. A* **95**, 012128 (2017).

[56] J. Johansson, P. Nation, and F. Nori, Qutip: An open-source python framework for the dynamics of open quantum systems, *Comput. Phys. Commun.* **183**, 1760 (2012).

[57] K. Husimi, Some formal properties of the density matrix, *Proc. Phys. Math. Soc.* **22**, 264 (1940).

[58] F. Strocchi, Thermal states, in *Symmetry Breaking* (Springer Berlin Heidelberg, Berlin, Heidelberg, 2008) pp. 139–150.

[59] Y. Guryanova, S. Popescu, A. J. Short, R. Silva, and P. Skrzypczyk, Thermodynamics of quantum systems with multiple conserved quantities, *Nat. Commun* **7**, 12049 (2016).

[60] F. Reiter and A. S. Sørensen, Effective operator formalism for open quantum systems, *Phys. Rev. A* **85**, 032111 (2012).